Interface profiles and in-plane anisotropy in common anion type-I $Cd_{1-x}Mg_xTe/CdTe/Cd_{1-x}Mn_xTe$ heterostructures studied by reflectivity

A. Kudelski, A. Golnik, and J. A. Gaj
Institute of Experimental Physics, Warsaw University, 69 Hoża, 00-681 Warszawa, Poland

F. V. Kyrychenko, G. Karczewski, and T. Wojtowicz
Institute of Physics, Polish Academy of Sciences, Al. Lotników 32/46, 02-668 Warszawa, Poland

Yu. G. Semenov
Institute of Semiconductor Physics, Ukrainian Academy of Sciences, Kiev, Ukraine

O. Krebs and P. Voisin
Ecole Normale Supérieure, 24 rue Lhomond, 75005 Paris, France
(Received 30 December 2000; published 21 June 2001)

We report on the experimental study of the in-plane optical anisotropy of CdTe-based quantum wells with asymmetric barriers made of (Cd,Mg)Te or (Cd,Mn)Te ternary compounds. We observe a significant linear polarization of the fundamental excitonic transitions along the $\langle 110 \rangle$ directions. The measured polarization rates are analyzed in the framework of an envelope function theory incorporating interface symmetry reduction for intermixed composition profiles. Fitting the experimental data produces interface anisotropy parameters that are larger than the ones predicted by a recent microscopic theory. The analysis shows an important influence of the interface profile asymmetry on the observed in-plane anisotropy.

DOI: 10.1103/PhysRevB.64.045312 PACS number(s): 78.20.Fm, 78.20.Jq

I. INTRODUCTION

The characterization of buried semiconductor heterointerfaces, in terms of compositional profile along the growth axis and roughness in the layer plane, has been the topic of intense interest for many years. However, the effect of microscopic symmetry reduction associated with a sharp chemical gradient, the associated heavy- and light-hole mixing at the minizone center and the corresponding in-plane optical anisotropy were discovered only recently. Among others, the interface symmetry reduction should be very important for transport of spin polarized carriers across interfaces, a crucial issue in the rapidly emerging field of spintronics. The results of the studies performed so far suggest that polarization-resolved spectroscopy under normal incidence has a strong potential for the nondestructive optical characterization of interfaces at a subnanometer length scale. Yet, in spite of its promises, this new spectroscopic tool has still not been implemented to clarify practical situations, and there remain open questions concerning the relation between material parameters and mixing of hole states at ideal or nonideal interfaces.

The comparison attempted here of heterostructures including several asymmetric single quantum wells aims at proving the direct correlation between growth sequences and observed optical anisotropy, and at obtaining quantitative results that can help clarify the above-mentioned fundamental issues. The cubic point-group symmetry T_d of a bulk zinc-blende semiconductor is reduced to the lower C_{2v} symmetry at an abrupt interface grown along the [001] axis. The C_{2v} symmetry cannot be accounted for when representing the interface by a one-dimensional step function $Y(z-z_{\mathrm{int}})$ that has a full rotational symmetry, as usually done in the classical envelope function theory (EFT). Instead, as first discussed by Ivchenko *et al.*,[1] the Hamiltonian must contain an interface term proportional to the lowest symmetry invariant of the C_{2v} group. A similar theory was discussed independently by Krebs and Voisin,[2] based on the consideration of the localization of valence band Bloch functions with respect to the atomic positions. The interface term couples the heavy- and light-hole states at the minizone center $k_t=0$. It can be handled in practice by generalizing the boundary conditions for the hole envelope functions, or diagonalized directly as a perturbation in the classical EFT eigenstates. The mixing of heavy- and light-hole states of the same symmetry (for instance, the ground states H1 and L1) gives rise to in-plane optical anisotropy. When considering a quantum well (QW), one has to combine the effects of at least two interfaces. A standard common-anion quantum well (such as $GaAs\text{-}Al_xGa_{1-x}As$) with ideally abrupt interfaces has a higher symmetry (D_{2d}) than a single interface, and has optical properties that are isotropic with respect to the in-plane direction of polarization. However, if the QW has some asymmetry, left and right interface terms do not compensate and some in-plane anisotropy appears. Possible causes are the existence of specific interface bonds, as in the case of ''no-common atom'' (NCA) QW's, more generally an asymmetry (deliberate or unintentional) of the composition profile, or the presence of an external electric field. Here we shall focus on a common-anion system based on CdTe QW's surrounded by different barriers, (Cd,Mn)Te and (Cd,Mg)Te. We present experimental investigations of their optical anisotropy as well as a theoretical calculation of light-hole–heavy-hole mixing at nonabrupt heterointerfaces.

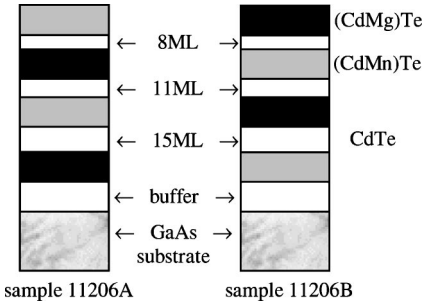

FIG. 1. Structure of the studied samples.

II. SAMPLES AND EXPERIMENTAL SETUP

The samples were grown on (100) GaAs substrates by molecular beam epitaxy at the Institute of Physics of Polish Academy of Sciences in Warsaw. Measurements were performed on two similar samples (Fig. 1). Sample 11206A contains three CdTe quantum wells 15-, 11-, and 8-monolayer (ML) wide (in the growth order), deposited on a 3-μm CdTe buffer followed by a $Cd_{1-x}Mg_xTe$ barrier. The quantum wells are separated by alternating barriers of $Cd_{1-x}Mn_xTe$ and $Cd_{1-x}Mg_xTe$ in such a way that the 15-ML and 8-ML wells have $Cd_{1-x}Mg_xTe$ barriers on the substrate side and the ones made of $Cd_{1-x}Mn_xTe$ on the opposite side, whereas for the 11-ML QW the order is reversed. The last $Cd_{1-x}Mn_xTe$ barrier serves as a cap layer. Mn and Mg concentrations are the same (i.e., $x=47\%$). Sample 11206B has a nominally identical structure, except that the order of $Cd_{1-x}Mn_xTe$ and $Cd_{1-x}Mg_xTe$ barriers is reversed. It is noteworthy that both the alloy band gaps and the valence band offsets at the $Cd_{1-x}Mg_xTe$-CdTe and $Cd_{1-x}Mn_xTe$-CdTe interfaces have similar values, so that from the EFT point of view, these quantum wells should be close to symmetric. The samples have been previously characterized[3] by magnetoreflectivity, the magnetooptical Kerr effect, and photoluminescence excitation. In order to determine interface profiles the spin tracing method has been applied, producing interface width values of about 3 Å for both CdTe/$Cd_{1-x}Mn_xTe$ and CdTe/$Cd_{1-x}Mg_xTe$ interfaces. The details of this characterization can be found in Ref. 3. One of the samples was also prepared for transmission measurements. It was glued to a glass plate and the opaque GaAs substrate was removed by an appropriate selective etching. Transmission spectra exhibited fine structures associated with the excitonic transitions in the different QW's (see further Fig. 2), but because of in-plane strain introduced by this procedure, the sample thus prepared was inadequate for anisotropy investigation. Therefore we chose reflectivity as our main experimental method, while using the transmission spectrum to confirm the identification of the excitonic ground state transitions in the various quantum wells. Absolute crystallographic orientation of the samples was determined by etching[4,5] of the rear side of the GaAs substrate in 1:8:1 volume mixture of 95% H_2SO_4, 30% H_2O_2, and H_2O. The etching revealed a groove pattern along the [110] direction on the substrate face. Assuming that the epitaxial layers reproduce the orientation of the substrate, we have concluded that the [110] direction on the surface of the heterostructure is perpendicular to the etched groove pattern on the back (in what follows we assume the growth direction to be [001]). Polarization-resolved reflectivity measurements were performed at 1.8 K. Strain-free mounted samples, immersed in superfluid helium, were illuminated by nonpolarized white light at nearnormal incidence. The source was a tungsten halogen lamp. A linear polarizer was placed in the light beam reflected from the sample. A 0.25-m grating spectrograph with a charge-coupled device matrix detector was used. Reflectivity spectra were recorded as a function of the linear analyzer angular position. The angles were measured related to the [110] direction of the samples. A careful selection of the elements of the experimental setup and a precise tuning is essential to reduce the influence of possible perturbing factors. A foil polarizer was chosen and the light spot on the spectrograph entrance slit was slightly defocused to reduce intensity changes caused by a possible displacement of the spot during rotation of the polarizer. The polarizer rotation axis was adjusted to coincide with the axis of the light beam to reduce the influence of any inhomogeneity of the polarizer. Grating spectrographs are known to exhibit a strong linear polarization. A circular polarizer with very weak spectral dependence was placed in front of the spectrograph to reduce the influence of this effect. The light emitted by a tungsten lamp is also slightly polarized. This polarization, estimated at about 10% in our experiment, is weakly wavelength dependent. As explained in the following, its influence was eliminated in the data processing.

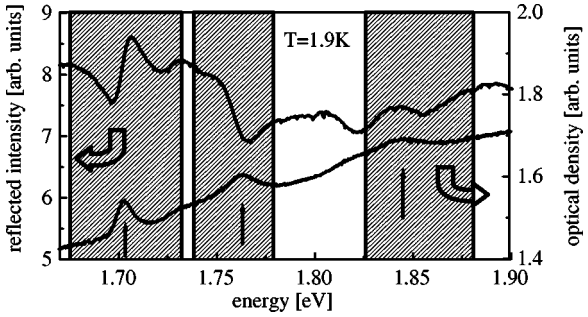

FIG. 2. Reflected intensity spectrum of sample 11206A (upper curve), averaged over all the angular positions of the analyzer, and optical density spectrum (lower curve) obtained by transmission measurement. Positions of $e1$-$h1$ transitions and photon energy ranges selected for fitting are marked by arrows and shadowed areas, respectively.

III. RESULTS AND QUALITATIVE ANALYSIS

Reflected signal measurements were carried out at linear analyzer angles ranging from 0° to 360° with a step of 30°. Figure 2 shows the reflected intensity obtained by averaging the different spectra over all the angular positions φ of the analyzer. For comparison, the optical density spectrum obtained by transmission measurement on a sample from the same wafer is also shown. Three absorption lines (positions marked by arrows) and corresponding reflectivity structures are identified as the $e1$-$h1$ excitonic transitions of the three different quantum wells. In order to analyze the dependence

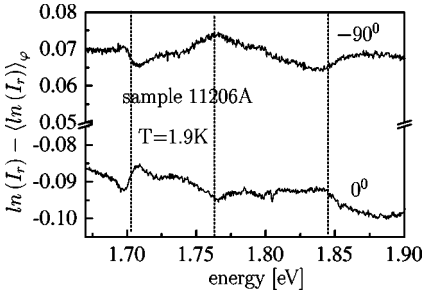

FIG. 3. Difference between logarithm of individual spectra and that of the averaged one for two particular analyzer angles (indicated).

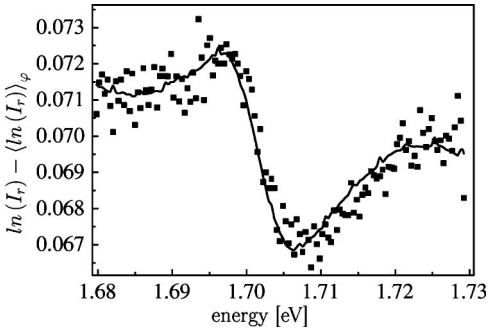

FIG. 4. Anisotropy spectrum of sample 11206A for $\varphi = 270°$ (dots) and its fit performed according to Eq. (1) (solid line). The fitted value is $A(\varphi) = -0.038$.

on φ of the spectra, we represent the reflectivity $R = I_r / I_0$ as a sum of resonant structures δR and a slowly varying background: $R = R_0 + \delta R$. I_r and I_0 denote intensities of reflected and incident light, respectively. The rapidly varying part δR corresponds to the resonant contribution of the $e1$-$h1$ excitonic transitions that is liable to present some optical anisotropy $\delta R = \langle \delta R \rangle_\varphi [1 + A(\varphi)]$, where $\langle \cdots \rangle_\varphi$ denotes the average over the angle φ. Furthermore, we assume that the amplitude of δR is proportional to the oscillator strength of the $e1$-$h1$ transitions. In case of linearly polarized reflectivity the relative variation $A(\varphi)$ will have the form

$$A(\varphi) = A_0 \cos(2\varphi), \tag{1}$$

where the amplitude A_0 gives the degree of polarization of these transitions. Our analysis includes also the residual polarization P defined as any polarization besides that coming from the quantum well excitonic transitions. By considering the logarithm of the reflected intensity I_r we obtain in a linear approximation:

$$\ln(I_r) - \langle \ln(I_r) \rangle_\varphi = P(\varphi) + \frac{\langle \delta R \rangle_\varphi}{R_0} A(\varphi). \tag{2}$$

In such differential spectra, the slowly varying contribution is attributed to the polarization background P of the setup, whilst the rapid and resonant contributions are attributed to the corresponding QW's. Figure 3 shows two examples of such anisotropy spectra obtained for the analyzer angles $0°$ and $-90°$. As expected [see Eqs. (1) and (2)], the two spectra are approximately opposite in sign. They clearly show excitonic structures in the spectral regions of the QW fundamental transitions over a flat background corresponding to P. In order to get a quantitative description of these results we have performed an empirical fitting of these structures. The idea was to make use of the different spectral dependencies of the two contributions of Eq. (1). For each of the three QW transitions, the first step was to choose an appropriate photon energy range. The latter should contain the reflectivity structure of interest, while cutting off any other optical transitions, such as $2S$ exciton states, light-hole transitions, etc. Within these limitations, the spectral range should be as wide as possible, to improve the accuracy of the fitting procedure. The selected ranges are marked in Fig. 2. As the trial function for the shape of the excitonic structures we have simply used the average logarithm of the reflected intensity I_r that contains the actual rapid contribution $\langle \delta R \rangle_\varphi / R_0$. The spectral dependence of the residual polarization P was chosen as a second degree polynomial to reduce the influence of any perturbations slowly varying with photon energy. Spectral fits (as shown on Fig. 4) were performed for each angle separately, producing $A(\varphi)$. Figure 5 shows that $A(\varphi)$ is closely fitted by the expected sinusoidal dependence [Eq. (1)]. The values of anisotropy amplitude A_0 obtained from fits of the experimental data are indicated in the figure.

Before we present a theoretical interpretation of these results, we first emphasize and comment briefly the main trends observed here. (1) We first note that all the amplitudes A_0 are positive. This means that the main contribution to the optical anisotropy does not originate from the difference of materials between the two barriers of a QW, but is inherent to the type of interface: normal (ternary grown on binary) or

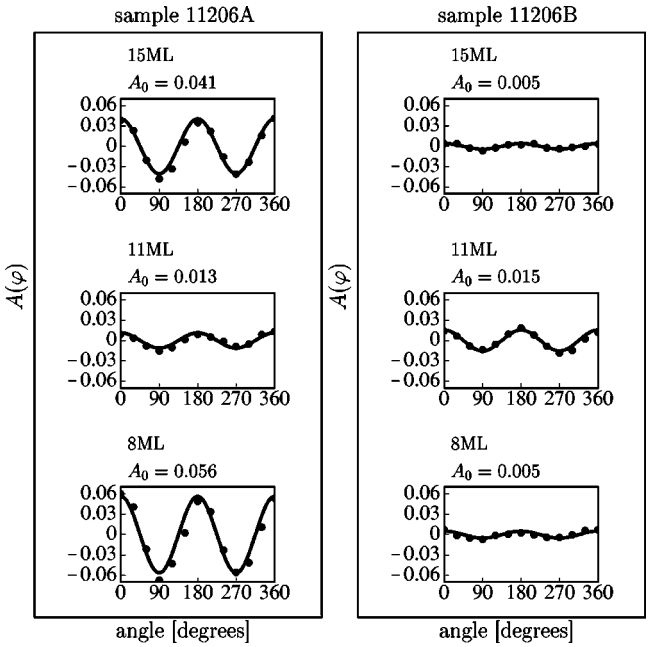

FIG. 5. Relative angular variation $A(\varphi)$ of excitonic reflectivity structures in the quantum wells of the two studied samples for the different analyzer angles φ. The solid lines represent theoretical dependence $A_0 \cos(2\varphi)$ with indicated amplitude values.

inverted (binary on ternary). As an example, the 11-ML QW of sample A exhibits an optical anisotropy similar to the 8- and 15-ML QW's of the same wafer, although the growth sequence of the barriers is opposite. In the following, this asymmetry is attributed to exponential composition profiles at the interfaces in agreement with previous spin tracing measurements on these samples.[3] (2) Quantum wells with (Cd, Mg)Te barriers on the substrate side and (Cd, Mn)Te alloy for the top barrier show a stronger anisotropy as compared to those grown in the reverse order. This is particularly obvious if we compare the three different QW's of a given sample. According to our analysis this property is due to the chemical asymmetry between the opposite interfaces of a QW. It contributes to the anisotropy with a different sign depending on the growth order and thus slightly increases or decreases the main anisotropy contribution given here by some asymmetrical potential. Three possible origins of that chemical difference can be addressed: (i) the substitution of a Cd atom by a Mn one creates a stronger intrinsic contribution to the anisotropy than the substitution of Cd by Mg, (ii) the Mn mole fraction in the (Cd,Mn)Te barriers is greater than that of Mg in (Cd,Mg)Te ones, and (iii) The CdTe/(Cd,Mn)Te interface is different (roughness, intermixing) from the CdTe/(Cd,Mg)Te one. Since the characterization of the samples[3] did not provide any indications in support of cases (ii) or (iii), we think that the first reason is the most probable one. (3) The measured amplitudes are systematically larger in sample A. The 11-ML QW of sample B has a stronger anisotropy than the other QW's of sample B, in agreement with the above-mentioned property. But it is not high enough to follow the regular and expected increase of anisotropy from the 15- to 8-ML wide QW's of sample A due to the reduction of the QW width. Therefore, this systematic discrepancy in the size of the effects must be related to a better structural quality of sample A (e.g., smaller interface roughness). This is not in contradiction with the similar intermixing lengths as determined in Ref. 3 (see the discussion of the roughness issues in Ref. 6). In what follows we propose a coherent quantitative description based on a simple envelope function theory where heavy- and light-hole mixing induced by the interfaces and more generally by any change of chemical composition, is taken into account. This gives support to the present qualitative analysis of these results.

IV. MODEL DESCRIPTION OF INTERFACE ANISOTROPY

For a theoretical description of the obtained results we generalize the approach used so far. It has been introduced by Ivchenko, Kaminski, and Rössler[1] (IKR), who used the elegant method of invariants and represented the asymmetry of the interface by suitable boundary conditions. An equivalent method known as H_{BF} model, proposed by Krebs and Voisin,[2] used projection of the valence wave functions on the interface bonds, more directly relating the anisotropy to its physical origin. We shall start here from the IKR approach. The boundary conditions for the envelopes can be represented by δ-shaped potentials placed at interfaces. Choosing J_z eigenfunctions as follows,

$$\Psi_{3/2}=(1/\sqrt{2})(X+iY)\uparrow,$$

$$\Psi_{1/2}=(1/\sqrt{6})(X+iY)\downarrow-\sqrt{\tfrac{2}{3}}Z\uparrow,$$

$$\Psi_{-1/2}=-(1/\sqrt{6})(X-iY)\uparrow-\sqrt{\tfrac{2}{3}}Z\downarrow,$$

$$\Psi_{-3/2}=-(1/\sqrt{2})(X-iY)\downarrow,$$

we obtain these potentials in the form

$$V_{int}=\pm\frac{i\hbar^2}{2m_0a}t\,\delta(z-z_0)\begin{pmatrix}0&0&1&0\\0&0&0&1\\-1&0&0&0\\0&-1&0&0\end{pmatrix}, \qquad (3)$$

for an interface placed at $z=z_0$, where the dimensionless coefficient t characterizes the anisotropy of the interface and signs plus or minus correspond to inverted or normal interface respectively, m_0 is the free electron mass, and a is the lattice constant. For a quantum well with identical barriers in a common-anion system the contributions from both interfaces compensate each other and excitons confined in the quantum well exhibit no in-plane anisotropy. In our case we should introduce two values of the dimensionless anisotropy coefficient: t_{Mn} for the CdTe/(Cd,Mn)Te interface and t_{Mg} for the CdTe/(Cd,Mg)Te one. We use CdTe lattice constant $a=6.48$ Å. Such a description would be clearly insufficient in our case since it predicts equal absolute values of contributions of the normal and inverted interfaces to the anisotropy, in contradiction with the experimental results. Therefore we introduce a generalized approach, taking into account a realistic composition profile at the interface. The anisotropy potentials that in the above-described model are localized at a perfectly sharp interface, will be now distributed over the interface profile range. This distribution can be expressed as a sum of δ-shaped potentials placed between consecutive monolayers; we chose a continuous description in which the term $\pm\delta(z-z_0)$ in Eq. (3) is replaced by the gradient $\partial p/\partial z$ of the interface profile $p(z)$ normalized as follows: $|p(\infty)-p(-\infty)|=1$. Note that the opposite sign of the gradient at the two interfaces of a quantum well takes over the task of the plus/minus sign of the Eq. (3). For the description of the light- and heavy-hole valence band states we use a simple band model with respective effective masses. The Schrödinger equation of a hole confined in a quantum well with the anisotropy represented by Eq. (3) separates in two identical equations in subspaces $\Psi_{-3/2}$, $\Psi_{1/2}$ and $\Psi_{3/2}$, $\Psi_{-1/2}$. We find eigenstates by solving numerically the set of two differential equations using an adaptive step size Runge-Kutta method, starting from a point in a barrier. We fit two parameters of the procedure, the energy and the initial ratio of the two components of the wave function to obtain vanishing wave functions, for $z\rightarrow\pm\infty$. Using the thus obtained valence wave functions Ψ_v, as well as the electron wave functions Ψ_e obtained by standard numerical

TABLE I. Parameters of the samples with measured (A_0^{expt}) and calculated (A_0^{theor}) polarization degree. Results of simplified calculations in the rectangular quantum well model without (A_0^{RQW}) and with ($A_0^{\text{RQW}+V_d}$) interface correction are shown for comparison. The intermixing length l_d is defined as the parameter of the exponential profile shape $P(z)=\Theta(z)[1-\exp(-z/l_d)]$ where $\Theta(z)$ is the Heaviside function.

Sample	Well width (ML) from Ref. 3	Intermixing length (Å) from Ref. 3	t_{Mn}	t_{Mg}	Polarization degree A_0^{expt}	A_0^{theor}	A_0^{RQW}	$A_0^{\text{RQW}+V_d}$
	14.9	3.5			0.041	0.046	0.029	0.046
11206A	11	3.8	2.076	2.028	0.013	0.011	-0.035	-0.014
	7.7	2.9			0.056	0.052	0.045	0.070
	13.7	3.5			0.005	0.007	-0.004	0.003
11206B	10.1	3.1	1.507	1.492	0.015	0.014	0.005	0.015
	7.5	3.4			0.005	0.003	-0.007	0.004

solution of scalar electron Schrödinger equation, we compute the electric dipole matrix elements for both linear polarizations

$$D^{\pm}=\langle\Psi_e|(1/\sqrt{2})(X\pm Y)|\Psi_v\rangle. \tag{4}$$

We calculate the degree of linear polarization as the relative difference of the squares of absolute values of these matrix elements

$$A_0=\frac{|D^+|^2-|D^-|^2}{|D^+|^2+|D^-|^2}. \tag{5}$$

Using exponential interface profiles corresponding to a segregation mechanism (see Ref. 7) we obtain indeed a nonvanishing anisotropy even in case of a quantum well with both barriers chemically identical. Assuming that the amplitude of the measured reflectivity structure is proportional to the square of the absolute value of electric dipole matrix element, we can compare directly the computed anisotropy with the experimental value defined in Eq. (1). For numerical computations we used parameters of Ref. 3 (see also Table I), where the quantum wells of our samples have been characterized. An example of the used potentials and obtained wave functions is presented in Fig. 6. Comparing the A_0 values obtained from our model with the experimental ones we determined two values of coefficient t for each sample, as shown in Table I. By using only two fitting parameters t_{Mn} and t_{Mg} we obtained a good agreement of the calculated anisotropy with experimental data. For both samples the obtained values of t_{Mn} are slightly larger than those of t_{Mg}. For comparison we present also in the Table I results of calculations performed for a rectangular quantum well (RQW) with perfectly sharp interfaces. We can see that the anisotropy alternates its sign depending on the growth order of the two barriers. This effect, due to the relation $t_{\text{Mn}}>t_{\text{Mg}}$, is suppressed by the interface broadening. Because of the asymmetric interface profile shape the interface mixing produces an effective shift of the wave function toward the normal interface, that determines the sign of A_0, as discussed in Sec. III. A simplified description of the interface profile effect on the anisotropy can be obtained by incorporation in the the RQW model of interface nonequivalence in the form of diagonal δ potentials $V_d\delta(z-z_0)$ that should be added to interface mixing term V_{int} [Eq. (3)]. A simulation of interface properties by δ-shaped potentials has been successfully used before for a description of Zeeman effect in CdTe/(Cd,Mn)Te heterostructures.[8] We treat V_d as a fitting parameter that reflects the deviation of interface potential from rectangular profile. Thus, interface potential amplitudes for normal (V_n) and inverted (V_i) interfaces may differ. The main function of these parameters is to shift the wave function toward one of the interfaces. Therefore it is the difference between them that is essential for the result. For this reason we introduce only one fitting parameter $V_d=V_n=-V_i$, identical for all the quantum wells in both samples. The best fitting to experimental data is reached for $V_d=30$ meV Å using the same anisotropy coefficients t_{Mn} and t_{Mg} as in the above-mentioned calculations. Results are presented in the last column of Table I. One can see that the δ-potential model for the interface can provide a reasonable quantitative description of optical anisotropy despite a number of simplifications. While producing a nice fit of the experimental results, the values obtained for t_{Mg}, t_{Mn} are anomalously large with respect to the values ($t\sim 0.2$) predicted[2,9] from the Krebs and Voisin H_{BF} model. The dis-

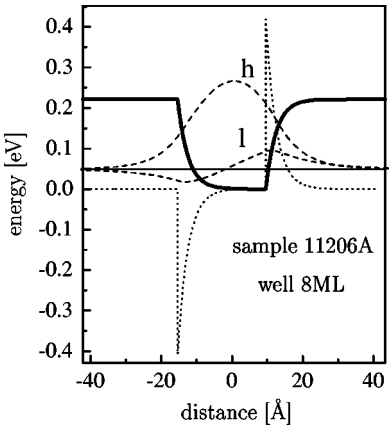

FIG. 6. Example of the calculation; solid line, diagonal quantum well potential; dotted line, off-diagonal mixing potential (imaginary part); dashed line, heavy- (*h*) and light- (l) hole wave function components (in arbitrary units).

crepancy may reflect the failure of that theoretical approach, or indicate that other phenomena come into play in these samples. Among others, the possibility of oriented corrugation[10] at the interfaces should be considered, as well as the possible presence of a built-in electric field due to the pinning of the Fermi level at the sample surface. It is also likely that, given the rather ionic character of the II-VI compounds, the bulk inversion asymmetry associated with the asymmetry of the well potential produces a significant contribution to the observed anisotropy.[11] More generally, the anisotropy of nearly symmetrical wells results from a small difference of large individual interface contributions, and may depend sensitively on details of the interface description. Atomistic calculations for the present system would help the elucidation of this point.

V. CONCLUSIONS

The experimental study of asymmetrical CdTe-based QW's has revealed a significant in-plane polarization anisotropy of the fundamental $e1$-$h1$ excitonic transitions. Since no change of sign occurred when reversing the growth sequence, we have concluded that the observed effects are not governed by an intrinsic difference of hole mixing coefficients (responsible for this anisotropy) at supposedly ideal interfaces. Instead, our data rather suggest that intermixing chemical profiles at the interfaces produce a stronger asymmetry of the potential for each QW that governs the optical anisotropy. The role of the ternary alloys of the barriers containing either the Mg or Mn species consists thus only in a certain modulation of this anisotropy when the growth sequence is reversed. These conclusions are confirmed by a theoretical calculation of hole mixing, where the interfaces are described by exponentially decreasing (or increasing) chemical composition of the ternary compound over a characteristic length of 3.5 Å. The recent model of localized C_{2v} mixing term in the EFT potential has been generalized to such profiles and provided a good fit of the whole set of experimental results. Here we have used the composition profile as an information given by previous experiments and then determined the interface parameters by fitting the amplitude of the optical anisotropy. However, since their amplitude seems to be one order of magnitude larger than the values predicted by a recent pseudopotential description of this coupling, it seems difficult to exclude a significant contribution of additional mechanisms such as surface electric field and bulk inversion asymmetry.

ACKNOWLEDGMENTS

This work was partially supported by the Polish Committee for Scientific Research (Grant No. 2 P03B 036 19), by French-Polish Collaboration Program Polonium, and by Grant No. INTAS-99-15.

[1] E.L. Ivchenko, A. Kaminski, and U. Rössler, Phys. Rev. B **54**, 5852 (1996).
[2] O. Krebs and P. Voisin, Phys. Rev. Lett. **77**, 1829 (1996).
[3] A. Lemaître, C. Testelin, C. Rigaux, S. Maćkowski, N.T. Khoi, J.A. Gaj, G. Karczewski, T. Wojtowicz, and J. Kossut, Phys. Rev. B **57**, 4708 (1998).
[4] S.D. Mukherjee and D.W. Woodard, in *Gallium Arsenide Materials, Devices and Circuits*, edited by M.J. Howes and D.V. Morgan (Wiley, New York 1986), p. 119.
[5] J. Woodward, in *Gallium Arsenide for Devices and Integrated Circuits*, edited by H. Thomas, D.V. Morgan, B. Thomas, J.E. Aubrey, and G.B. Morgan, Vol. 3 of the IEEE Electrical and Electronic Materials and Devices Series (IEEE, London, 1986), p. 144.
[6] W. Grieshaber, C. Bodin, J. Cibert, J.A. Gaj, Y. Merle d'Aubigné, A. Wasiela, and G. Feuillet, Appl. Phys. Lett. **65**, 1287 (1994).
[7] J.A. Gaj, W. Grieshaber, C. Bodin-Deshayes, J. Cibert, G. Feuillet, Y. Merle d'Aubigné, and A. Wasiela, Phys. Rev. B **50**, 5512 (1994).
[8] J. Siviniant, F.V. Kyrychenko, Y.G. Semenov, D. Coquillat, D. Scalbert, and J.P. Lascaray, Phys. Rev. B **59**, 10 276 (1999).
[9] S. Cortez, O. Krebs, and P. Voisin, European Phys. J. B (to be published).
[10] D. Gammon, E.S. Snow, B.V. Shanabrook, D.S. Katzer, and D. Park, Phys. Rev. Lett. **76**, 3005 (1996).
[11] E.L. Ivchenko, A.A. Toropov, and P. Voisin, Fiz. Tverd. Tela (St. Petersburg) **40**, 1925 (1998) [Phys. Solid State **40**, 1748 (1998)].